Received: 30 June 2023 | Revised: 13 May 2024 | Accepted: 2 June 2024

DOI: 10.1002/hbm.26761

RESEARCH ARTICLE

WILEY

Changes of brain parenchyma free water fraction reflect tissue damage and impaired processing speed in multiple sclerosis

Alessandra Stella Caporale[1,2] | Antonio Maria Chiarelli[1,2] | Emma Biondetti[1,2] | Alessandro Villani[1,2] | Ilona Lipp[3] | Davide Di Censo[1,2] | Valentina Tomassini[1,2,4,5] | Richard Geoffrey Wise[1,2,5]

[1]Department of Neuroscience, Imaging and Clinical Sciences, 'G. d'Annunzio University' of Chieti-Pescara, Chieti, Italy

[2]Institute for Advanced Biomedical Technologies (ITAB), 'G. d'Annunzio University' of Chieti-Pescara, Chieti, Italy

[3]Department of Neurophysics, Max Planck Institute for Human Cognitive and Brain Sciences, Leipzig, Germany

[4]MS Centre, Department of Clinical Neurology, 'SS. Annunziata' University Hospital, Chieti, Italy

[5]Cardiff University Brain Research Imaging Centre (CUBRIC), School of Psychology, Cardiff University, Cardiff, UK

Correspondence
Alessandra Stella Caporale, Department of Neuroscience, Imaging and Clinical Sciences, 'G. d'Annunzio University' of Chieti-Pescara, Chieti, Italy.
Email: alessandra.caporale@unich.it

Funding information
European Union's Horizon Europe Research and Innovation Program, Grant/Award Number: 101066055; European Union - NextGenerationEU- Italian Ministry of University and Research (MUR), National Plan for Recovery and Resilience (PNRR) and Projects of National Relevance (PRIN), Grant/Award Numbers: P20225AEEE, P2022ESHT4, 2022BERM2F; National Recovery and Resilience Plan (NRRP), Grant/Award Number: ECS00000041

Abstract

Free water fraction (FWF) represents the amount of water per unit volume of brain parenchyma, which is not bound to macromolecules. Its excess in multiple sclerosis (MS) is related to increased tissue loss. The use of mcDESPOT (multicomponent driven single pulse observation of T1 and T2), a 3D imaging method which exploits both the T1 and T2 contrasts, allows FWF to be derived in clinically feasible times. However, this method has not been used to quantify changes of FWF and their potential clinical impact in MS. The aim of this study is to investigate the changes in FWF in MS patients and their relationship with tissue damage and cognition, under the hypothesis that FWF is a proxy of clinically meaningful tissue loss. To this aim, we tested the relationship between FWF, MS lesion burden and information processing speed, evaluated via the Symbol Digit Modalities Test (SDMT). In addition to standard sequences, used for T1- and T2-weighted lesion delineation, the mcDESPOT sequence with 1.7 mm isotropic resolution and a diffusion weighted imaging protocol ($b = 0$, 1200 s/mm^2, 40 diffusion directions) were employed at 3 T. The fractional anisotropy map derived from diffusion data was used to define a subject-specific white matter (WM) atlas. Brain parenchyma segmentation returned masks of gray matter (GM) and WM, and normal-appearing WM (NAWM), in addition to the T1 and T2 lesion masks (T1L and T2L, respectively). Ninety-nine relapsing–remitting MS patients (age = 43.3 ± 9.9 years, disease duration 12.3 ± 7.7 years) were studied, together with twenty-five healthy controls (HC, age = 38.8 ± 11.0 years). FWF was higher in GM and NAWM of MS patients, compared to GM and WM of HC (both $p < .001$). In MS patients, FWF was the highest in the T1L and GM, followed by T2L

Valentina Tomassini and Richard Geoffrey Wise contributed equally to this study.

and NAWM, respectively. FWF increased significantly with T1L and T2L volume (ρ ranging from 0.40 to 0.58, $p < .001$). FWF in T2L was strongly related to both T1L volume and the volume ratio T1L/T2L ($\rho = 0.73$, $p < .001$). MS patients performed worse than HC in the processing speed test (mean ± SD: 54.1 ± 10.3 for MS, 63.8 ± 10.8 for HC). FWF in GM, T2L, perilesional tissue and NAWM increased with SDMT score reduction ($\rho = -0.30, -0.29, -0.33$ respectively and $r = -.30$ for T2L, all with $p < .005$). A regional analysis, conducted to determine which NAWM regions were of particular importance to explain the relationship between FWF and cognitive impairment, revealed that FWF spatial variance was negatively related to SDMT score in the corpus callosum and the superior longitudinal fasciculus, WM structures known to be associated with cognitive impairment, in addition to the left corticospinal tract, the sagittal stratum, the right anterior limb of internal capsule. In conclusion, we found excess free water in brain parenchyma of MS patients, an alteration that involved not only MS lesions, but also the GM and NAWM, impinging on brain function and negatively associated with cognitive processing speed. We suggest that the FWF metric, derived from noninvasive, rapid MRI acquisitions and bearing good biological interpretability, may prove valuable as an MRI biomarker of tissue damage and associated cognitive impairment in MS.

KEYWORDS
cognitive impairment, damage, free water fraction, MRI, multiple sclerosis, relaxation

Practitioner Points

1. The fraction of unbound water (free water fraction [FWF]) in relapsing–remitting multiple sclerosis (MS) patients exceeds that of healthy controls, as a consequence of the structural changes occurring in the brain parenchyma at the expense of the nervous tissue.
2. FWF in MS patients reflects lesion burden in terms of volume of T1-hypointense and T2-hyperintense lesions and correlates with information processing speed measured through the Symbol Digit Modalities Test.

1 | INTRODUCTION

Multiple sclerosis (MS) is characterized by variable degrees of demyelination, axonal loss, gliosis, microglial activation and blood–brain barrier (BBB) disruption. These processes concur to alter brain parenchyma, where spontaneous repair mechanisms may not cope with the structural damage (Compston & Coles, 2008; Saade et al., 2018). The structural changes brought about by MS are accompanied by alterations of motor and cognitive functions, the latter having a prevalence of up to 65%, involving mainly memory, sustained attention and information processing speed (Amato et al., 2006; Sumowski et al., 2018).

MS damage is most evident in lesions, localized in the white matter (WM) and in the gray matter (GM) (Filippi et al., 2012; Tomassini & Palace, 2009). In the WM, lesions manifesting on MRI as T2 hyperintensities (T2 lesions, T2L) may present axonal loss and matrix destruction, appearing on MRI as T1 hypointensities (T1 lesions, T1L) (Sahraian et al., 2010; Tomassini & Palace, 2009; van Waesberghe et al., 1998). T1L load is more closely related to disability (quantified via the Expanded Disability Status Scale [EDSS]; Kurtzke, 1983) than T2L load (Valizadeh et al., 2021). Also, the tissue away from the lesion's edges is only "normal-appearing," as it differs substantially from healthy tissue and presents microglial activation, axonal pathology, and myelin loss (Filippi et al., 2012).

During the development of tissue damage, several pathophysiological mechanisms tend to replace the nervous tissue by cerebrospinal fluid (CSF) and/or extracellular fluid: (i) where myelinated axons have been degraded beyond repair, water fraction increases due to an expansion of the extracellular space or water influx from the damaged BBB (Sahraian et al., 2010); (ii) a "tissue shift" with water replacement may be due to atrophy, which occurs in MS from the early stages of the disease (Gentile et al., 2023); and (iii) enlarged perivascular spaces, the fluid-filled spaces that surround small vessels in the brain parenchyma, are more common in MS patients than in healthy controls

(HCs; Granberg et al., 2020), representing another potential source of water increase. The amount of water per unit volume, which is not bound to macromolecules, is referred to as the "free water fraction" (FWF). Considering the diffusivity of water molecules, FWF indicates the water pool that does not experience flow, nor restricted diffusion (Pasternak et al., 2009). In MS, FWF captures the additional water reservoir (additional with respect to myelin-trapped water, intra and extra-axonal water, and CSF), arising from other sources such as inflammation or edema. In a recent study a certain predictive value of FWF was reported, that is the capacity of baseline FWF to predict which T2-hyperintense lesions at baseline would atrophy at 5-year follow-up, reflecting thus the proportion of degraded nervous tissue replaced by free water (Bergsland et al., 2021).

The relaxation contrast method can be employed to quantify FWF with MRI. This method relies on the heterogeneous transverse relaxation properties of water: while water trapped between the lamellae of the myelin phospholipidic bilayer has a short T2 component (T2 $\sim$ 20 ms), the intra/extracellular water exhibit intermediate T2 relaxation times (50 ms < T2 < 100 ms), and the CSF and edema are associated with a long T2 component (T2 > 100 ms). An approach to quantify FWF, introduced originally for myelin water imaging, implements a multicompartmental analysis of T2-decay curves using spin echo acquisitions at multiple echo times (Laule et al., 2007; Mackay et al., 1994; Whittall et al., 1997). However, the long acquisition time and reduced signal to noise ratio at long echo times needed to map the free water component limit the applicability of this method for 3D imaging. An alternative approach replaces the multi-echo spin echo acquisition with a multi-flip angle balanced steady-state free precession (bSSFP) sequence (Deoni et al., 2003). However, the bSSFP is sensitive to both T2 and longitudinal (T1) relaxation, which itself changes as a function of the level of boundness of water. Hence, the bSSFP is coupled with a T1-sensitive multi-flip angle spoiled gradient echo (SPGR) in a method called mcDESPOT (multicomponent driven equilibrium single pulse observation of T1 and T2; Deoni et al., 2008, 2013). This method was shown to be three times more efficient than multi-point inversion recovery to derive T1, and then multi-echo spin-echo to derive T2, respectively (Deoni et al., 2003). McDESPOT permits 3D imaging of the whole brain in times compatible with the clinical protocols without sacrificing accuracy (Deoni et al., 2008). In its latest implementation, the mcDESPOT approach relies on a three-compartment model including three sub-voxel anatomical water pools: myelin-trapped water, intra/extra-axonal water and a free water compartment. However, the full potential of this rapid 3D imaging method has not yet been exploited to quantify FWF in MS.

Here, using the mcDESPOT technique, we verified that FWF of MS patients exceeded that of healthy subjects and investigated the relationship between this excess FWF and the extent to which a particular aspect of the cognitive domain, information processing speed, was impaired, under the hypotheses that a higher FWF would correspond to a larger extent of brain tissue damage, and be associated with slower information processing speed.

2 | METHODS

2.1 | Study protocol

Demographic, clinical, and MRI data for the present study were taken from cohorts of MS patients and HCs, matched for age and sex, previously collected (Lipp et al., 2019, 2021). We included only relapsing–remitting MS (RRMS), right-handed individuals, whose clinical stability was ascertained by a follow-up visit, a month after the study. Patients were included only in case of no relapse or change in disease treatment within at least 3 months before the study entry.

Disease duration, EDSS score (Kurtzke, 1983) and level of education were recorded. Cognitive processing speed was evaluated by Symbol Digit Modalities Test (SDMT), one of the most sensitive task for cognitive monitoring in MS (Parmenter et al., 2007; Sumowski et al., 2018). The SDMT score registers the number of correct associations between symbols and digits in 90 s, based on a given reference key, with the numbers 1–9 corresponding to different geometric symbols. The test was administered to both patients and healthy subjects.

2.2 | MRI acquisition

An MRI protocol including T2/proton-density-weighted imaging, fluid-attenuated inversion recovery (FLAIR) for identification and segmentation of T2-hyperintense lesions (T2L), and a 1-mm-isotropic resolution T1-weighted (T1w) sequence for identification of T1-hypointense lesions (T1L) was performed at 3 T on a GE system (GE Medical Systems, Milwaukee, WI) using an eight channel receive-only head RF coil (Lipp et al., 2019). In addition, a mcDESPOT sequence with 1.7 mm-isotropic resolution and a diffusion-weighted protocol were acquired. For diffusion, a twice refocused diffusion-weighted sequence was used (to reduce the effect of eddy currents), with $b = 0$, 1200 s/mm^2, and 40 uniformly distributed diffusion gradient directions. Diffusion weighted images (DWIs) were used to produce maps of fractional anisotropy (FA) to normalize a standard WM atlas to the subjects' native space, in order to extract individual WM tracts. The parameters of the sequences used in the MRI protocol are listed in Table 1, and a diagram illustrating the steps of the mcDESPOT acquisition pipeline is provided in Figure 1.

2.3 | MRI data processing

A combination of FSL routines (FMRIB Software Library v6.0.4; Jenkinson et al., 2012) and in-house MATLAB scripts (MATLAB R2020b, The MathWorks Inc.) were used for data processing. The FWF maps were obtained with a combination of FSL routines, and in-house Python (v3.9) and bash scripts. Briefly, a three-pool model including a fast, slow, and very slow relaxing water (attributed to myelin, intra-extra axonal and bulk, free, non-exchanging water, respectively) is used to describe water relaxation and fitted to the data. The

TABLE 1 MRI protocol: details on sequence parameters.

	T2/PD-weighted	FLAIR	T1-weighted	mcDESPOT	DWI
Sequence acronym in GE	SE	SE-IR	FSPGR	SPGR, bSSFP, IR-SPGR	SE-EPI
In-plane resolution (mm^2)	0.94 × 0.94	0.86 × 0.86	1.0 × 1.0	1.72 × 1.72	1.80 × 1.80
Slice thickness (mm)	4.5 (3.0 + 1.5 gap)	4.5 (3.0 + 1.5 gap)	1.0	1.7	2.4
Number of slices	36	36	3D imaging	3D imaging	57
Field of view (mm^2)	240 × 240	220 × 220	256 × 256	220 × 220	230 × 230
Matrix size	256 × 256	256 × 256	256 × 256 × 172	128 × 128 × 88	128 × 128
Flip angle (°)	90	90	20	SPGR: (3, 4, 5, 6, 7, 8, 9, 13, 18) bSSFP: (10.6, 14.1, 18.5, 23.8, 29.1, 35.3, 45, 60) IR-SPGR: 5	90
$TE_{1,2}$/TR (ms)	9.0,80.6/3000	122.3/9502	3.0/7.8	SPGR: 2.1/4.7 bSSFP: 1.6/3.2 IR-SPGR: 2.1/4.7	94.5/16,000
TI (ms)	-	2250	450	IR-SPGR: 450	-
Acquisition time (min)	2	3	7.5	10	12.5

Abbreviations: bSSFP, balanced steady-state free precession; DWI, diffusion weighted imaging; EPI, echo-planar imaging; FLAIR, fluid-attenuated inversion recovery; FSPGR, fast spoiled gradient echo; GE, General Electric; IR, inversion recovery; mcDESPOT, multicomponent driven equilibrium single pulse observation of T1 and T2; SE, spin-echo; SPGR, spoiled gradient recalled-echo; TE, echo time; TI, inversion time; TR, repetition time.

longitudinal magnetization is modeled as a sum of three contributions for SPGR (only the longitudinal magnetization is considered, as the transverse magnetization is spoiled prior to each radiofrequency excitation pulse):

$$S_{SPGR} = M_{z,M}^{SPGR} + M_{z,IE}^{SPGR} + M_{z,F}^{SPGR} \quad (1)$$

The transversal magnetization is modeled as a sum of three contributions for bSSFP:

$$S_{bSSFP} = M_{x,M}^{bSSFP} + M_{x,IE}^{bSSFP} + M_{x,F}^{bSSFP} + i\left(M_{y,M}^{bSSFP} + M_{y,IE}^{bSSFP} + M_{y,F}^{bSSFP}\right) \quad (2)$$

where the subfixes M, IE, and F stand for myelin, intra-extra axonal water, and free water, respectively. Equations (1) and (2) are fit to acquired multiple flip angle data using a stochastic region contraction approach, as described in Deoni et al. (2013), allowing to derive estimates of 9 parameters: the relaxation times in the three compartments, $T_{1,M}$, $T_{1,IE}$, $T_{1,F}$, $T_{2,M}$, $T_{2,IE}$, $T_{2,F}$, the signal fraction of water in two compartments (myelin water fraction [MWF] and FWF, with the assumption that the intra-extra axonal fraction is IEF = 1 − (MWF + FWF)), and the mean residence time of water in myelin, tM. The present work focuses on the FWF only.

For the "global" analysis, the FWF maps were nonlinearly registered to the T1w-image (structural image) using Elastix (Klein et al., 2010; Lipp et al., 2019). The T1w-image was automatically segmented after lesion filling (Gelineau-Morel et al., 2012), combining FSL FAST and FIRST routines in a customized MATLAB script. FSL FAST segments the bias-field corrected structural image reporting partial volume estimates for the three tissue types (WM; GM; CSF): a specific voxel was assigned to one of these tissue types by selecting the tissue compartment with the highest partial volume. The FSL FIRST routine is designed to segment the subcortical GM nuclei. The combination of the two routines returned masks of "cortical plus subcortical" GM, as well as WM, which were eroded by one pixel to reduce partial volume errors. CSF was discarded, to focus the analysis on brain parenchyma. Brain tissue volume, normalized for subject head size, was estimated with SIENAX (Smith et al., 2002, 2004) from the high-resolution T1-weighted images, to estimate brain atrophy. Hyperintense T2 lesion masks (T2L-masks) were generated semi-automatically from FLAIR images using the Jim software package (v.6, Xinapse). Hypointense T1 lesion masks (T1L-masks) were derived as a subset of the T2L-masks, considering the voxels belonging to T2L-masks, with intensities lower than the average intensity of GM (van Walderveen et al., 2001). Lesion load was evaluated in terms of T1 and T2 lesion volume, measured in ml. T2L-masks were spatially dilated in 3D by 5 mm and subtracted from the WM-mask to obtain a mask of normal-appearing WM (NAWM). The difference between WM and NAWM, discarding the T2L-masks, constituted the perilesional tissue. Figure 2 illustrates the tissue masks generated within the WM of MS patients, together with a sample FWF map.

For the "regional" analysis, DWIs were skull stripped using BET and corrected for eddy current distortions using the EDDY routine, producing rotated *b*-vectors. Scalar invariant indices (mean diffusivity

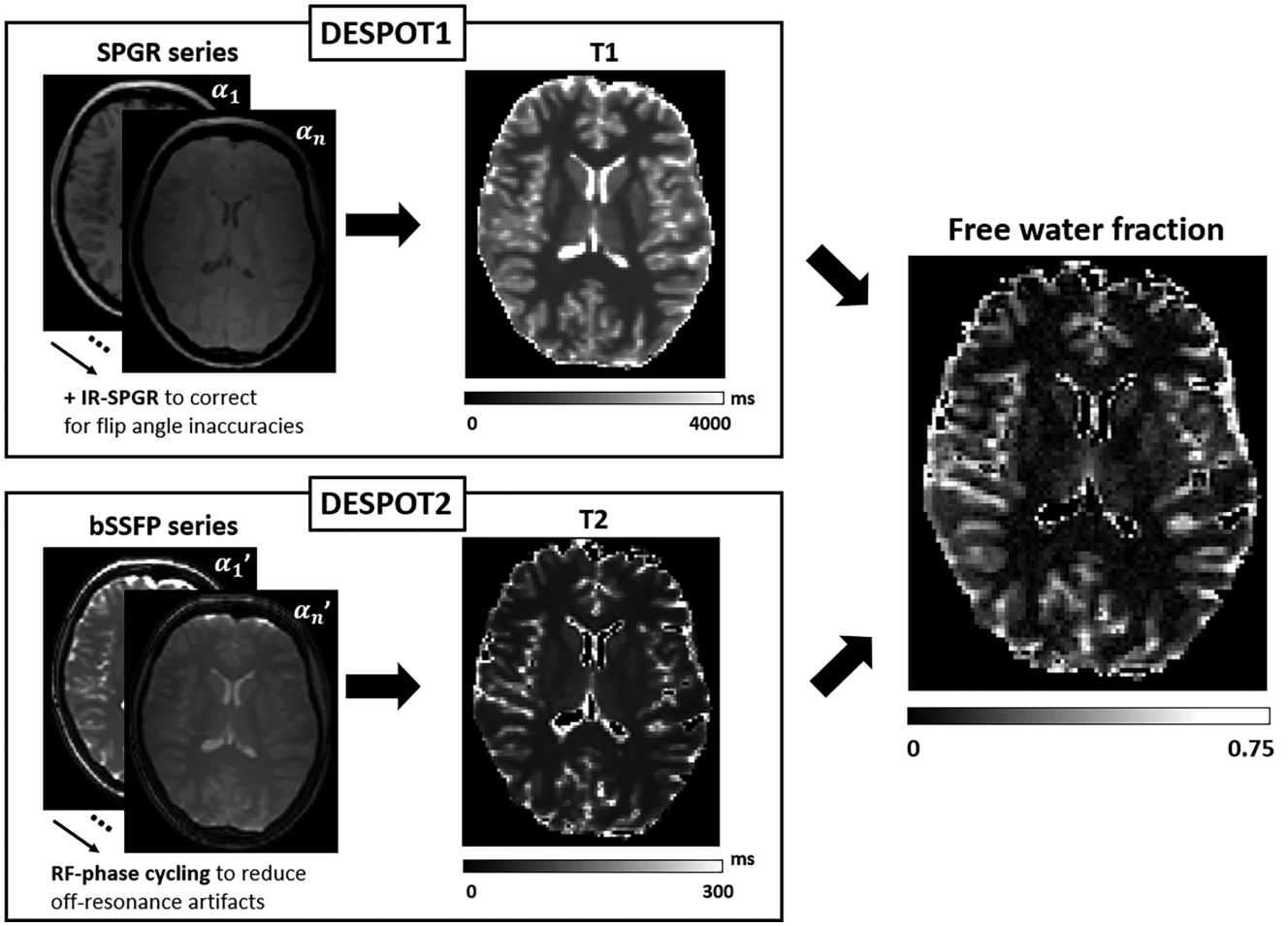

FIGURE 1 Diagram illustrating the mcDESPOT (multicomponent driven equilibrium single pulse observation of T1/T2) technique. McDESPOT combines DESPOT1 and DESPOT2 methods with a multicomponent, multi-compartment model of water relaxation. Quantitative maps of T1 and T2 are derived, respectively, by fitting spoiled-gradient echo (SPGR) and balanced steady-state free precession (bSSFP) signal intensities to varying flip angles (α_1... α_n, differing between DESPOT1 and DESPOT2). In DESPOT1, an inversion-recovery SPGR (IR-SPGR) is used for correction of B1 inhomogeneities (Deoni, 2007); in DESPOT2, the effect of B0 inhomogeneities is mitigated by the use of RF-phase cycling (Deoni et al., 2004). A three-pool model including a fast, slow and very slow relaxing water (attributed to myelin, intra-extra axonal and bulk, non-exchanging water, respectively) is used to describe water relaxation. A map of the fraction of free water is shown on the right.

[MD], axial diffusivity [AD], radial diffusivity [RD], FA) were extracted via DTIFIT using a weighted least square method for fitting and the rotated *b*-vectors returned by EDDY. The SPGR M_0 image was used as a reference to coregister the b0 image (image with no diffusion weightings) with an affine registration (12 degrees of freedom, trilinear interpolation, correlation ratio cost function). The inverse transformation was then used to map the FWF onto the DWI native space. A native WM atlas was obtained from the standard ICBM-DTI-81 WM labels atlas (Mori et al., 2005). First, native FA was linearly registered to the standard MNI space. The transformation matrix was used to initialize the nonlinear registration (FNIRT) using the FA as input and the JHU-ICBM-FA-1 mm atlas as reference. The obtained warping field was inverted and applied to the standard WM atlas (JHU-ICBM-labels-1 mm), returning a subject-specific WM atlas, which was then eroded by one pixel to mitigate partial volume errors. A total of 48 WM tracts or regions of interest (ROIs) were considered. An FA threshold of 0.3 was applied to exclude voxels including less coherent fiber tracts (Hasan et al., 2005). The regional analysis was conducted to see whether FWF changes in key WM regions (implicated in information processing speed, visual working memory and sustained attention, all cognitive domains involved in the execution of an SDMT test) would be associated with variation in SDMT performance.

2.4 | Statistical analysis

Sex distribution balance among MS and HC groups was tested via Pearson's Chi Square test in SPSS (IBM, SPSS statistics, v20.0.0). Differences in age and years of education between the two groups were assessed with independent *t* tests, with homogeneity of variances tested via Levene's test. Age and years of education were then considered as covariates when testing for differences in SDMT score between the two groups. FWF mean and variance were extracted from each GM, NAWM, perilesional tissue, T1L, and T2L mask. FWF

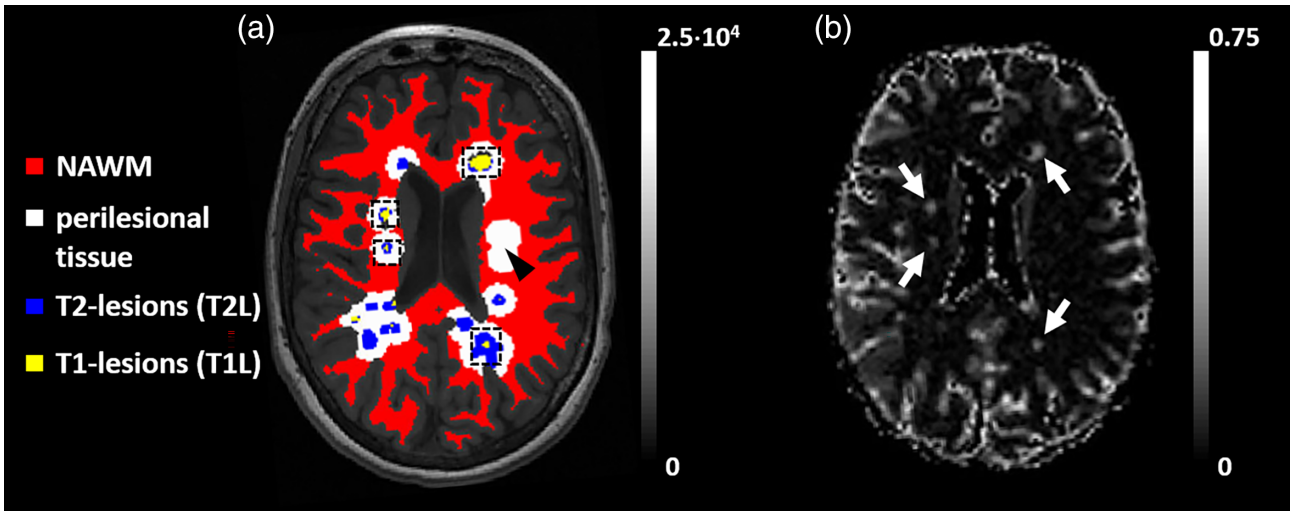

FIGURE 2 Tissue masks segmented within the white matter and free water fraction (FWF) map. (a) Normal appearing white matter (NAWM), perilesional tissue, T2-hyperitense lesions (T2L), T1-hyperintense lesion (T1L) masks are overlayed onto a T1-weighted structural map (color bar on the right, intensity units). Please note that the masks shown are two-dimensional cuts through a three-dimensional mask, which explains why the perilesional tissue on the right does not contain T2 or T1-lesions (arrowhead). (b) FWF map for the same slice shown in (a). White arrows point at four representative T1-lesions (highlighted with dashed boxes in panel a).

TABLE 2 Demographics for the healthy control subjects (HC) and the relapsing–remitting MS patients (RRMS).

	HC ($N = 25$)	RRMS ($N = 99$)	*p*-Value
F/M	13/12	68/31	.117[a]
Age (years)	38.8 ± 11.0[b] (23–59)	43.3 ± 9.9 (18–60)	.045
Education (years)	19.8 ± 4.3 (12–30)	15.9 ± 4.2 (10–30)	<.001
Disease duration (years)	-	12.3 ± 7.7 (1–39)	-
EDSS score[c]	-	2.0 (0–6.5)	-
SDMT score[d]	63.8 ± 10.8 (42–84)	54.1 ± 10.3 (31–81)	<.001; .002

Abbreviations: EDSS, Expanded Disability Status Scale; HC, healthy controls; RRMS, relapsing–remitting multiple sclerosis patients; SDMT, Symbol Digit Modalities Test.
[a]Pearson's Chi squared test with one degree of freedom = 2.454.
[b]Mean ± SD, range in parenthesis.
[c]EDSS was not available for 8 out of the 99 MS patients; median EDSS is reported.
[d]The second *p*-value shown refers to the test considering age and education as covariates.

variance provided a measure of FWF spatial heterogeneity. Since the FWF values were log-normally distributed within each tissue with the exception of T1L (where they were normally distributed), the mean and variance of the lognormal distribution were considered, instead of the arithmetic mean and standard deviation. In addition, FWF median and variance were extracted from 48 NAWM regions derived from the WM atlas. Normality of the distributions of tissue FWF in the two subject groups were tested with Lilliefors test performed in R (v. 4.2.1, *nortest* package; Gross & Ligges, 2015; R Core Team, 2022). A two-sided Wilcoxon rank sum test was used to assess differences in FWF and SDMT score between groups (MS vs HC), and the paired version of the test was used to assess differences in FWF between various tissues within the patient group. Pearson's r or Spearman's ρ (in case of non-normality) between FWF and the clinical data (lesion volume, lesion volume ratio, and SDMT score) were evaluated. Pearson's r between FWF of NAWM regions and SDMT was evaluated. False discovery rate adjusted p-values were calculated using the linear-step up procedure originally introduced by Benjamini and Hochberg (1995).

3 | RESULTS

3.1 | Demographic and clinical characteristics of the participants

Here, 99 RRMS patients (68/31 women/men, mean ± SD age = 43.3 ± 9.9 years) and 25 HC subjects (13/12 women/men, mean ± SD age = 38.8 ± 11.0 years) were included in the analysis. Demographic data are listed in Table 2. Sex distribution was not significantly different between the disease and control groups (see Table 2). RRMS patients had a disease duration of 12.3 ± 7.7 years (range 1–39 years), a median EDSS of 2.0 (range 0–6.5, with 88% of patients able to walk without any aid) and were slightly older ($p = .045$) and less educated

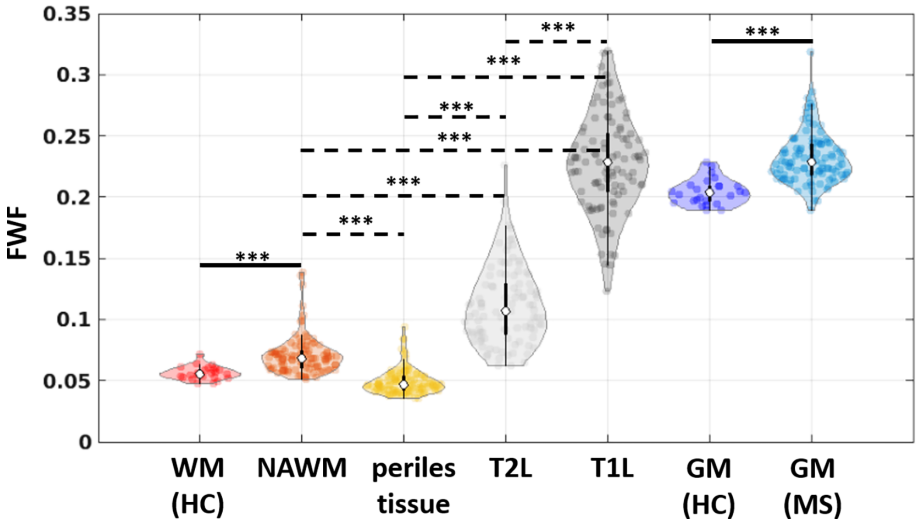

FIGURE 3 Violin plots of free water fraction (FWF) in brain tissues. FWF distribution in normal (healthy control, HC) and pathological (multiple sclerosis, MS) brain tissues. From left to right: white matter, WM; normal appearing white matter, NAWM; perilesional space, indicating an area of 5 mm around the T2-hyperintense lesions; T2-hyperintense lesions, T2L; T1-hypointense lesions, T1L; gray matter, GM. Black horizontal bars indicate significant differences between the two subject groups (thick bars), or significant paired tests within the patient group (dashed bars). *** $p < .001$.

than HC ($p < .001$). Older patients had a longer disease duration ($r = .46$, $p < .001$). Most patients (68%) were not receiving disease modifying therapy (DMT, see Supplementary Materials, Figure S1). As expected, MS patients performed worse than HC in the processing speed test (unadjusted mean ± SD: 54.1 ± 10.3 for MS, 63.8 ± 10.8 for HC; adjusted mean ± standard errors: 54.5 ± 1.0 for MS, 62.0 ± 2.1 for HC, adjusted $p = .002$, where age, but not years of education, showed a significant effect).

3.2 | Brain parenchyma FWF and its association with lesion burden

The distribution of FWF in the different tissues is depicted by the violin plot in Figure 3, with median values listed in Table S1 (Supplementary Materials). The violin plot reporting the FWF spatial heterogeneity can be found in Supplementary Materials, Figure S2. FWF was higher in GM and NAWM of MS patients, compared to GM and WM of HC, respectively (both $p < .001$, significant after outlier rejection, with no significant effects of age or years of education). Within MS patients FWF differed significantly among tissues ($p < .001$), except between GM and T1L ($p = .81$), and it was higher in the T1L and GM, followed by T2L and NAWM. Conversely, the perilesional tissue had the lowest FWF. Among the tissue types examined, FWF in T1L showed the largest variability across patients.

No correlations were found between FWF and age or years of education in any tissue. The correlation between FWF and lesion load, evaluated in terms of volumes of T1L and T2L, is depicted in Figure 4. The correlation plots between FWF variance in the various tissues and lesion load can be found in Supplementary Materials, Figure S3. FWF of GM, NAWM, and perilesional tissue were positively associated with WM lesion load, with Spearman's correlation coefficient ρ ranging from 0.40 to 0.58 ($p < .001$). Average FWF in T2L was strongly related to both T1L volume and the volume ratio T1L/T2L ($\rho = 0.73$, $p < .001$). All the correlations shown in Figure 4 were significant after the Bonferroni correction for multiple comparisons, except for the correlation between FWF in T1L and the T1L/T2L volume ratio (Figure 4h). For what concerns brain atrophy, rank-sum tests showed a significantly lower GM volume for MS patients compared to healthy subjects, while the WM volumes did not differ on a group-basis. In patients, the volume of brain parenchyma (sum of GM and WM volumes) showed a negative correlation with the volume of T1-hypointense lesions ($\rho = -0.30$, $p < .005$) and with the volume of T2-hyperintense lesions ($\rho = -0.26$, $p = .010$). This correlation was dominated by GM, indeed GM volume was related with the volume of T1 lesions and T2 lesions ($\rho = -0.34$, $p < .001$ and $\rho = -0.27$, $p < .01$), while WM volume was not. In MS patients, GM-FWF correlated significantly with GM volume, with $\rho = 0.51$, $p < .0001$. In contrast, neither GM-FWF nor WM-FWF correlated with WM volume.

3.3 | Brain parenchyma FWF and the information processing speed in MS patients

SDMT score showed a weak negative correlation with EDSS ($\rho = -0.23$, $p = .028$) and a moderate correlation with T1L and T2L volumes ($\rho = -0.33$, $p \leq .001$). In GM, NAWM, perilesional tissue and T2L, FWF increased with reduction of SDMT score ($\rho = -0.30$, -0.29, -0.33, respectively, and $r = -.30$ for T2L, all with $p < .005$, Figure 5). However, FWF was not related to EDSS in any of these tissues. The correlation between FWF variance in the distinct tissues and SDMT ranged from a maximum negative correlation of $r = -.35$ ($p < .0005$) for T1-hyperintense lesions, to a minimum negative correlation of $\rho = -0.23$ ($p < .05$) for T2 lesions, not significant after the correction for multiple comparisons.

With regard to the regional analysis, no significant correlations were found between FWF and SDMT in any of the considered WM tracts in the HC group. Conversely, several significant associations were found between FWF and SDMT score in the MS group. The

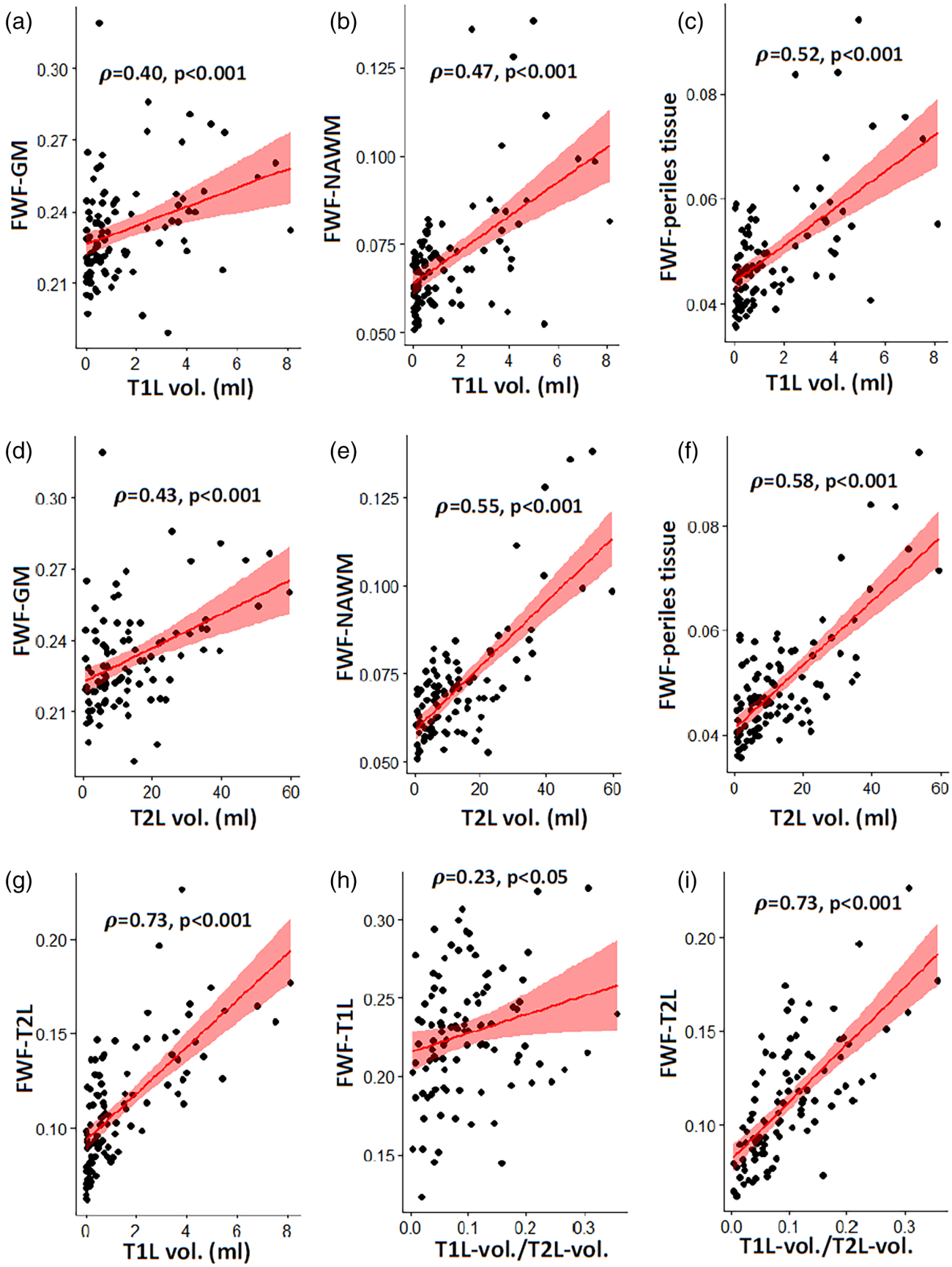

FIGURE 4 Legend on next page.

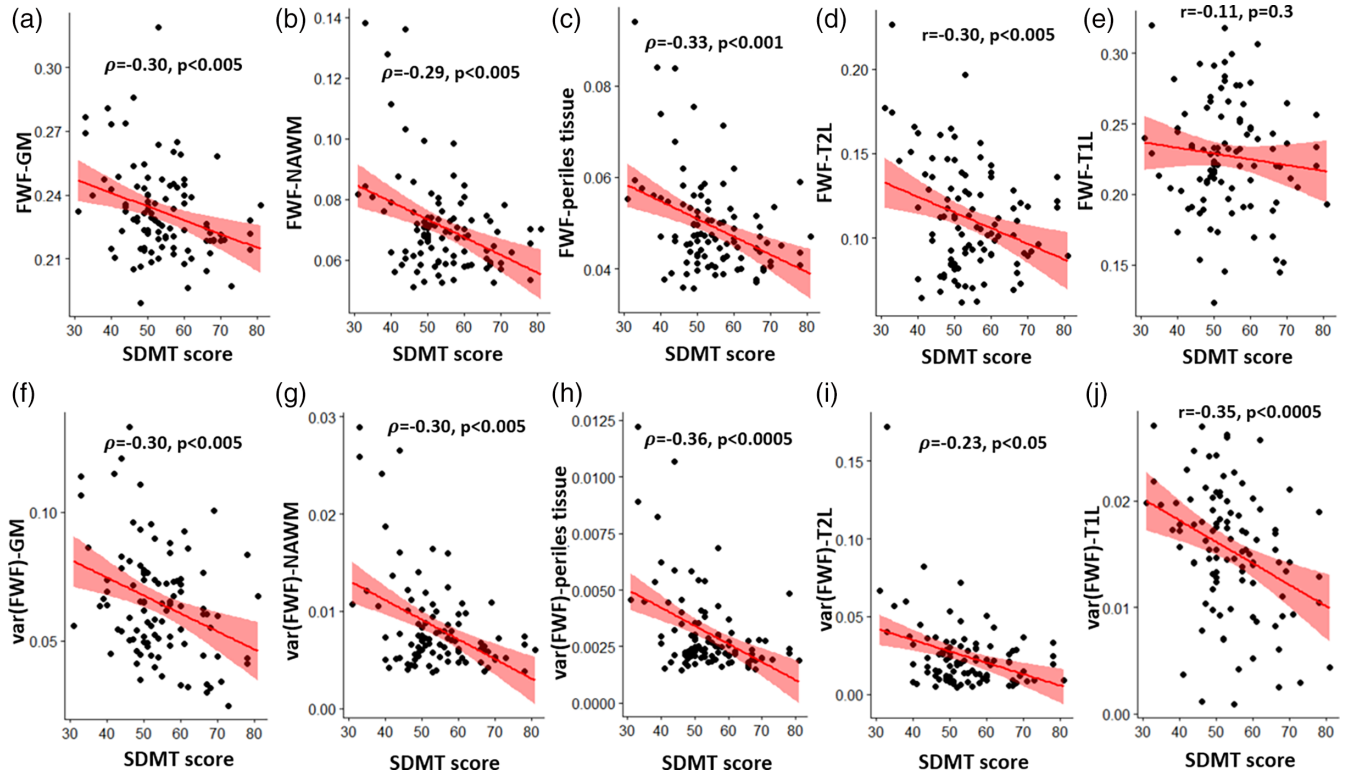

FIGURE 5 Scatterplots of brain parenchyma free water fraction (FWF) and symbol digit modalities test (SDMT) scores. Mean FWF (a–e) and FWF spatial variance (f–l) in gray matter (GM, a, f); normal appearing white matter (NAWM, b, g); perilesional tissue (c, h); T2-hyperintense (d, i); and T1-hypointense MS lesions (e, l) is plotted against the SDMT score for the cohort of relapsing–remitting MS patients. Spearman (ρ) or Pearson (r) correlation coefficients (where appropriate) are indicated, together with the significance level. Please, note that the correlation in (i) is not significant after correcting for multiple comparisons ($p' = .05/10 = 0.005$). The regression line and confidence intervals are also reported in red.

results of the correlation tests are summarized visually in Figure 6 and listed in Table S2 (Supplementary Materials). Both median FWF and FWF spatial variance were negatively related with SDMT score, with the correlation reaching statistical significance in five ROIs for median FWF (body of corpus callosum; anterior limb of internal capsule right [alic-R]; sagittal stratum right and left, including inferior longitudinal fasciculus and inferior fronto-occipital fasciculus; fornix/stria terminalis right).

FWF spatial variance in NAWM decreased with SDMT score in 16 ROIs in MS patients, including the genu and body of corpus callosum, corticospinal tract (cst) right and left (approaching significance for the first one), the sagittal stratum right and left, the superior cerebellar peduncle right, the alic-R, the superior longitudinal fasciculus (slf) right, approaching significance for slf-left (see Table S2 and Figure 6).

4 | DISCUSSION

This study quantified cerebral FWF in clinically stable RRMS and investigated its relationship with lesion burden and information processing speed. We used the mcDESPOT sequence, which allows rapid (<15 min) acquisition of whole brain, spatially resolved 3D imaging with simultaneous T1 and T2 relaxation mapping. We thus fitted a three-compartment relaxation model, with free water as the slowest-relaxing pool, to spoiled-gradient-echo and balanced-SSFP signals with varying flip angles (Deoni et al., 2013), obtaining FWF maps that are comparable across subjects.

The hypothesis that FWF in brain parenchyma of MS patients exceeded that of HC was verified in the global analysis. FWF was higher in both GM and NAWM compared, respectively, to GM and WM of control subjects. In MS patients, GM-FWF correlated

FIGURE 4 Scatterplots of brain parenchyma free water fraction (FWF) and lesion characteristics. Mean FWF in gray matter (GM, a, d); normal appearing white matter (NAWM, b, e); perilesional tissue (c, f); T1-hypointense and T2-hyperintense MS lesions (g–i) is plotted against T1 and T2 lesion volumes; and their ratio for the cohort of relapsing–remitting MS patients. Spearman's correlation coefficient ρ is indicated, together with the significance level p. Please, note that the correlation in (h) is not significant after correcting for multiple comparisons ($p' = .05/15 = 0.0033$). The regression line and confidence intervals are also reported in red.

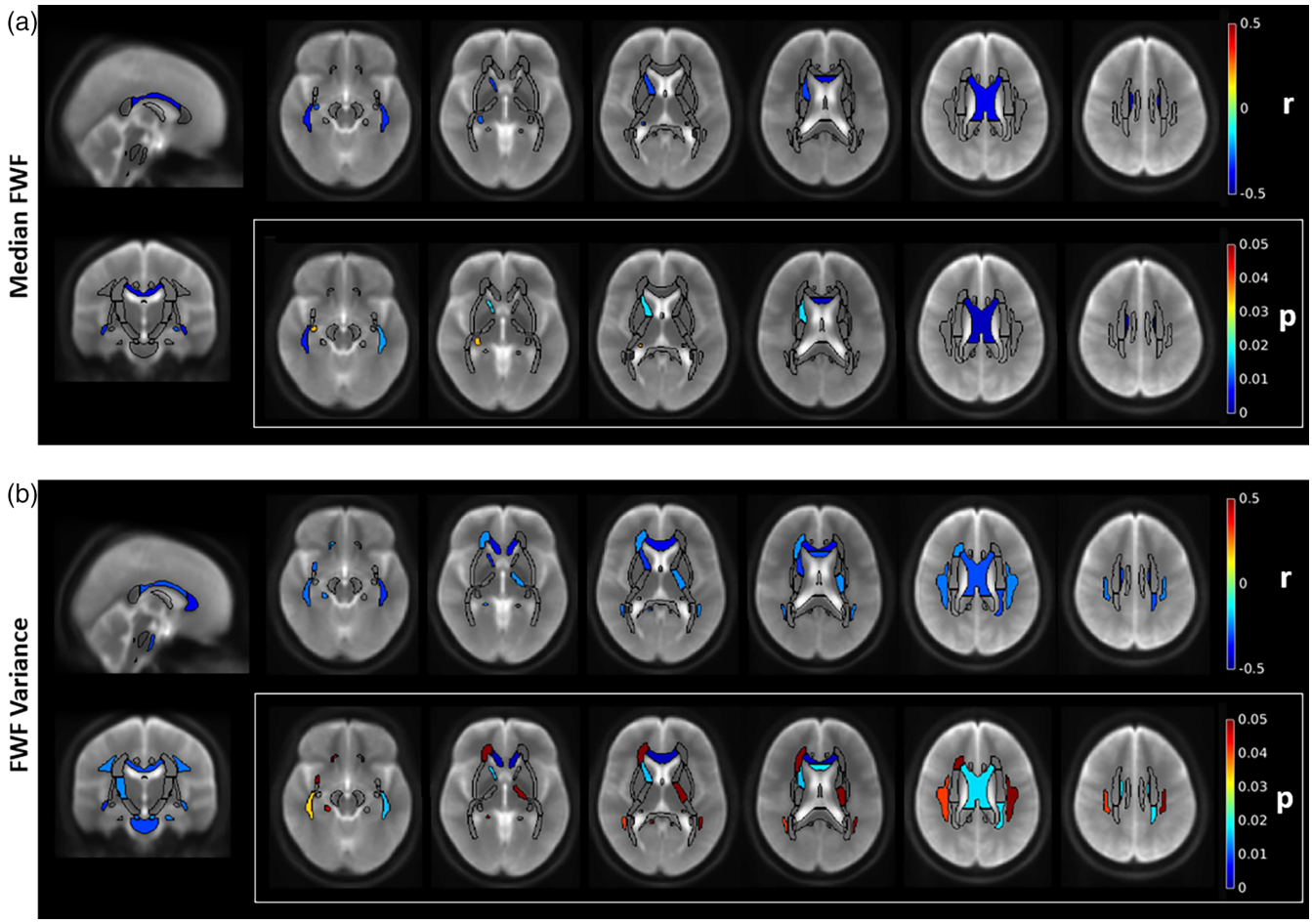

FIGURE 6 Relation between free water fraction (FWF) and symbol digit modality test (SDMT) score in MS patients. Pearson's correlation coefficient r between median FWF (a) or FWF spatial variance (b) and SDMT score is illustrated in white matter regions, with the respective *p*-value *p* (white box). Only regions where the correlation is significant after false discovery rate correction are shown in colors, overlayed on T2-weighted anatomical maps. Sagittal and coronal views are shown for *r*-maps for the sake of clarity.

significantly with GM volume, with $\rho = 0.51$, $p < .0001$, indicating that in patients with larger cerebral atrophy (lower GM volume) the GM had a larger proportion of free water. In contrast, neither GM-FWF nor WM-FWF correlated with WM volume.

The highest content of FWF was found in the T1-hypointense lesions, the portion of brain parenchyma where nervous tissue degradation is prominent. The fact that MS patients showed greater FWF than HC can be explained considering several peculiar processes of the MS pathology: an augmented water influx due to BBB damage, an expanded extracellular space due to inflammatory edema, a "tissue shift" due to atrophy (Saade et al., 2018). The fact that FWF of NAWM was significantly higher than that of WM in HCs is consistent with observations that this tissue is affected by various degrees of pathology in MS, ranging from microglial activation without axonal pathology to axonal involvement and myelin loss (Filippi et al., 2012). Instead, the area surrounding T2 lesions (i.e., the perilesional tissue) showed a significantly lower FWF than both lesions and NAWM, possibly due to distinct pathophysiological processes occurring in this area. For example, a perilesional accumulation of inflammatory cells (Frischer et al., 2009) could reduce the content of free water by hiding myelin damage; in addition, a certain degree of remyelination with rescuing of perilesional space signal (Ricigliano et al., 2022) could alter FWF in this tissue.

Interestingly, FWF was associated with MS lesion burden, evaluated in terms of T1L and T2L volumes, with greater volume of lesioned tissue corresponding to a higher FWF (Figure 4). FWF of NAWM and perilesional tissue showed stronger correlations with lesion load compared to the volume of brain parenchyma (as the sum of GM and WM volumes) and to the GM and WM volumes taken singularly. In particular, we found that FWF of T2-hyperintense lesions was strongly related to both T1L volume and T1L/T2L volume ratio, which may suggest a dependence of FWF on the proportion of T2L that is also T1-hypointense, or in other words, on the proportion of T2L that potentially underwent axonal loss and matrix destruction. In a different study, FWF in T2L evaluated at baseline proved to be predictive with respect to which T2L would be affected by a process of atrophy at 5-year follow-up (Bergsland et al., 2021). In addition, in the study by Laule et al., MS patients with longer disease duration exhibited T2 lesions with an increased fraction of a "long-T2" water component, which was negatively associated with the MWF, underlying

the link between structural changes such as demyelination and increased water content (Laule et al., 2007). Considering these findings, FWF may be a useful addition to the toolbox of MRI parameters for the assessment of MS disease progression.

Given that FWF is associated with the degree of nervous tissue alteration in MS, it follows that it could be associated also with the functional changes brought about by MS. Cognitive dysfunction, evaluated by means of neurobehavioral tests, can be present from the earliest stages of the disease. It is, however, not necessarily reflected in the EDSS, a score used to summarize the neurological status of MS patients, which is heavily weighted toward the physical disability. Conversely, moderate to strong correlations between the degree of cognitive dysfunction and total cerebral lesion load can be found (Amato et al., 2006). In our study, we considered the SDMT as a tool to measure the performance in a specific cognitive domain, the information processing speed. Among the various tests, the SDMT is most sensitive in MS with respect to the cognitive processing speed, likely because good performance depends on multiple functions affected by MS (mostly processing speed, but also memory and visual scanning) (Sumowski et al., 2018). The SDMT score obtained by RRMS patients in our cohort (54.1 ± 10.3) was lower than that of control subjects, as expected. Moreover, FWF in MS patients was associated with SDMT in the different tissues and in several WM tracts. In another study where FWF was evaluated by exploiting the diffusion contrast via the free water elimination method at 3 T, a group of 24 RRMS patients scored 62.1 ± 8.1 in the oral version of the SDMT test (Beaudoin et al., 2021). Global lesion load was not associated with the neuropsychological performance and no correlation was found between FWF of selected WM tracts and SDMT. This lack of correlation was ascribed to the young age of patients (29 years), their short disease duration (4.3 years, range 0.4–12 years) and limited EDSS scale (median = 1.5, range 0–3.0). By comparison, our cohort presented a longer disease duration (12.3 ± 7.7 years, range 1–39 years), and a larger EDSS range (median = 2.0, range 0–6.5). However, differences in the results could also be because evaluating FWF by exploiting the relaxation contrast, rather than the diffusion contrast, might be sensitive to different aspects of the tissue microstructural changes brought about by MS.

In the regional analysis, we found that FWF variance (representing its spatial heterogeneity) increased with worsening SDMT performance (lower SDMT score) in the corpus callosum and in the superior longitudinal fasciculus of MS patients. Conversely, no association was found between SDMT and FWF median or spatial variance in the brain parenchyma of HC subjects. Previous studies found a similar association between MWF variance and SDMT score in the corpus callosum, superior longitudinal fasciculus and cingulum of MS patients (Abel et al., 2020), and some WM abnormalities (evaluated in terms of decreased FA) in the corpus callosum, superior longitudinal fasciculus, anterior limb of internal capsule of RRMS patients with cognitive impairment (established based on their performance on SDMT and Paced Auditory Serial Addition Test) (Zhang et al., 2017). Taken together, these results may indicate that the higher the structural heterogeneity of WM regions, in terms of MWF and FWF, the larger the impact on the processing speed performance, as evaluated by the SDMT, suggesting that FWF may reflect the degree of functional damage.

In the current study, we obtained quantitative maps of brain parenchyma FWF using the time-efficient, 3D imaging mcDESPOT method, which is based on the water relaxation contrast. This method has been employed for MWF quantification by some of the present co-authors, in the same cohort of RRMS patients and additional primary progressive MS patients, showing good performance in differentiating T2-hyperintense lesions from NAWM (Lipp et al., 2019).

However, the FWF can be estimated also with a different approach, i.e., by exploiting the contrast provided by water diffusion in the various tissue compartments. This approach fits a bi-tensorial model to diffusion weighted (DW) data, which isolates the isotropic contribution to the diffusion contrast of freely diffusing water from that of restricted water (Pasternak et al., 2009). This method, also known as "free water elimination," was originally introduced to correct for CSF and edema-related contamination of diffusion tensor metrics (Pierpaoli & Jones, 2004), and it is reliable, provided that the DW protocol includes at least two non-zero b-shells (Golub et al., 2021; Hoy et al., 2014). Conversely, the application of this approach to single non-zero *b*-value DW data (like those acquired in our MRI protocol) requires strong regularizations and constraints on diffusivities and volume fractions to solve an ill-posed problem, and caution in the interpretation of results (Golub et al., 2021). A systematic study comparing the two metrics (FWF evaluated through relaxation and the diffusion contrast) in the same group of subjects is currently missing, according to our knowledge. For completeness purposes, we investigated the correlation between SDMT and FWF evaluated from our diffusion data acquired with a single *b*-shell. We used the code publicly available at https://github.com/mvgolub/FW-DTI-Beltrami, which employs the Beltrami regularization and produces parametric maps of free water, and tissue-specific MD and FA. The results of this analysis can be found in the Supplementary Materials, Table S3, and showed a lower number of significant associations in NAWM for MS patients, compared to mcDESPOT-derived FWF (see also Supplementary File to view a comparison between the two parametric maps for a representative control subject). Moreover, it is worth mentioning that despite sharing the same name, the two parameters, mcDESPOT-FWF and diffusion-based FW do not represent the exact same physical properties of tissues. While Pasternak's model considers essentially two water diffusion compartments, tissue water (comprising intracellular water, water in the myelin lamellae, and thus water at the interface between the intracellular and extracellular space) and extracellular water (comprising extracellular water and the free water), mcDESPOT considers three compartments based on the T1 and T2 relaxation properties of water: myelin-trapped water, water in the intra and extracellular space, and free water.

Our work presents some limitations. First, we segmented the T1w-image to derive masks of the different tissue types. In the present study, voxels with a partial volume estimate of CSF higher than the WM and GM were excluded. In the original paper where mcDESPOT was first introduced, the parenchyma tissue was defined as that

containing less than 10% CSF (Deoni et al., 2008). Therefore, the adopted criterion can underestimate the fraction of CSF and overestimate the brain parenchyma. This was mitigated in the current work by the use of mask erosion. To reduce partial volume artifacts with CSF, voxels with a partial volume value of CSF higher than 30% had been previously excluded from the T2L masks (Bergsland et al., 2021). We verified that in our study, over 99.5% voxels in the T2L masks belonged to brain parenchyma. A second limitation is represented by the mixed profile of treatments in our MS cohort: 32 out of 99 participants were on DMTs, when they were enrolled. It is unclear how the DMTs could alter FWF in brain parenchyma. Clarifying this aspect would require a longitudinal study. A third limitation is the spatial resolution of FWF maps, currently around $1.7 \times 1.7\ mm^2$, which does not allow to study the contribution of enlarged perivascular spaces to the increased FWF in patients (for which an in-plane resolution of at least $0.9 \times 0.9\ mm^2$ would be needed; Piantino et al., 2020). Finally, in this work, we focused on a particular functional domain, the information processing speed. However, the relationship between FWF accumulation and the other functional domains not investigated here, such as motor function or visuospatial capabilities, would be worth further investigation.

5 | CONCLUSIONS

Alterations of brain structure in MS are associated with replacement of tissue by free water. This process not only involved MS lesions within the WM, but also the NAWM and the GM, impinging on brain function and negatively affecting processing speed. FWF, that is water content per unit volume in brain parenchyma, and its spatial variation, especially in NAWM, may be a marker of tissue damage and associated cognitive impairment in MS. The use of the mcDESPOT method to obtain a full volumetric brain coverage, yielding simultaneously maps of MWF and FWF in clinically feasible times, allows broader monitoring of the evolution of MS over time.

AUTHOR CONTRIBUTIONS

Conceptualization: R.G.W., V.T., A.S.C., and A.M.C. Methodology: A.S.C., R.G.W., A.M.C., E.B., and V.T. Software: A.S.C. Validation: A.S.C., A.V., and A.M.C. Investigation: A.S.C. and I.L. Data curation: A.S.C. Writing—original draft preparation: A.S.C. and A.M.C. Writing—review and editing: A.S.C., A.M.C., E.B., A.V., I.L., V.T., and R.G.W. Revisions: A.S.C., D.d.C., and A.M.C. Bids formatting: D.d.C. Visualization: A.S.C. Supervision: R.G.W. Funding acquisition: R.G.W., V.T., and A.S.C. All authors have read and agreed to the published version of the manuscript.

ACKNOWLEDGMENTS

The authors would like to thank the Helen Durham Centre for Neuroinflammation, University Hospital of Wales, Cardiff, UK for patient recruitment, and the volunteers who participated in this study.

FUNDING INFORMATION

This study was supported by the MS Society UK; it was partially conducted (ASC) under the framework of the Departments of Excellence 2018–2022 initiative of the Italian Ministry of Education, University and Research for the Department of Neuroscience, Imaging and Clinical Sciences (DNISC) of the University of Chieti-Pescara, Italy, and funded by the "Fund for the Promotion and Policy Development of the National Research Programme (PNR)" (Decree n. 737/2021); it was supported (AMC) by the European Union—NextGenerationEU-Italian Ministry of University and Research (MUR), Research National Program (PNR) and Projects of National Relevance (PRIN), Project Code: 2022BERM2F, Project Title: "Mapping Mitochondrial Function and Oxygen Metabolism in the Human Brain with Magnetic Resonance Imaging." Funding call No. 104 of 02.02.2022, Concession decree No. 1065 of 18.07.2023 adopted by MUR, ERC Panel LS7 "Prevention, Diagnosis and Treatment of Human Diseases." CUP: D53D23013410001 and by the European Union—NextGenerationEU-Italian Ministry of University and Research (MUR), National Plan for Recovery and Resilience (PNRR) and Projects of National Relevance (PRIN), Project Code: P20225AEEE, Project Title: "Hybrid PET-MRI to simultaneously probe brain metabolism and cerebrovascular function in neurodegenerative diseases." Funding call No. 1409 of 14.09.2022, Concession decree No. 1369 of 01.09.2023 adopted by MUR, ERC Panel LS7 "Prevention, Diagnosis and Treatment of Human Diseases." CUP: D53D23021480001; it was supported by (ASC, DDC and RW) the European Union—NextGenerationEU under the National Recovery and Resilience Plan (NRRP), Mission 4 Component 2—M4C2, Investment 1.5—Call for tender No. 3277 of 30.12.2021 Italian Ministry of University Award Number: ECS00000041, Project Title: "VITALITY—Innovation, digitalization and sustainability for the diffused economy in Central Italy," Concession Degree No. 1057 of 23.06.2022 adopted by the Italian Ministry of University, CUP: D73C22000840006; it was supported (EB) by the European Union's Horizon Europe research and innovation programme under the Marie Skłodowska-Curie grant agreement No 101066055—acronym HERMES. Views and opinions expressed are however those of the author(s) only and do not necessarily reflect those of the European Union or the European Research Executive Agency (REA). Neither the European Union nor the granting authority can be held responsible for them; it was supported (ASC, VT and RW) by the European Union—NextGenerationEU-Italian Ministry of University and Research (MUR), National Plan for Recovery and Resilience (PNRR) and Projects of National Relevance (PRIN), Project Code: P2022ESHT4, Project Title: "Advancing MRI biomarkers of brain tissue microstructure and energetics in Multiple Sclerosis." Funding call No. 1409 of 14.09.2022, Concession decree No. 1367 of 01.09.2023 adopted by MUR, ERC Panel LS5 "Neuroscience and Disorders of the Nervous System." CUP: D53D23019210001.

CONFLICT OF INTEREST STATEMENT

The authors have no conflicts of interest to disclose.

DATA AVAILABILITY STATEMENT

The data presented in this study are available on request from the corresponding author (BIDS Validator v1.14.5). The code and scripts are published in a public mcDESPOT_FWF_MS repository.

ORCID

Alessandra Stella Caporale https://orcid.org/0000-0002-2182-8312
Antonio Maria Chiarelli https://orcid.org/0000-0002-5347-8417

REFERENCES

Abel, S., Vavasour, I., Lee, L. E., Johnson, P., Ackermans, N., Chan, J., Dvorak, A., Schabas, A., Wiggermann, V., Tam, R., Kuan, A. J., Morrow, S. A., Wilken, J., Laule, C., Rauscher, A., Bhan, V., Sayao, A.-L., Devonshire, V., Li, D. K., … Kolind, S. H. (2020). Myelin damage in normal appearing white matter contributes to impaired cognitive processing speed in multiple sclerosis. *Journal of Neuroimaging*, *30*(2), 205–211. https://doi.org/10.1111/jon.12679

Amato, M. P., Zipoli, V., & Portaccio, E. (2006). Multiple sclerosis-related cognitive changes: A review of cross-sectional and longitudinal studies. *Journal of the Neurological Sciences*, *245*(1), 41–46. https://doi.org/10.1016/j.jns.2005.08.019

Beaudoin, A.-M., Rheault, F., Theaud, G., Laberge, F., Whittingstall, K., Lamontagne, A., & Descoteaux, M. (2021). Modern technology in multi-shell diffusion MRI reveals diffuse white matter changes in young adults with relapsing-remitting multiple sclerosis. *Frontiers in Neuroscience*, *15*, 1008. https://doi.org/10.3389/fnins.2021.665017

Benjamini, Y., & Hochberg, Y. (1995). Controlling the false discovery rate: A practical and powerful approach to multiple testing. *Journal of the Royal Statistical Society: Series B (Methodological)*, *57*(1), 289–300. https://doi.org/10.1111/j.2517-6161.1995.tb02031.x

Bergsland, N., Dwyer, M. G., Jakimovski, D., Weinstock-Guttman, B., & Zivadinov, R. (2021). Diffusion tensor imaging reveals greater microstructure damage in lesional tissue that shrinks into cerebrospinal fluid in multiple sclerosis. *Journal of Neuroimaging*, *31*(5), 995–1002. https://doi.org/10.1111/jon.12891

Compston, A., & Coles, A. (2008). Multiple sclerosis. *The Lancet*, *372*(9648), 1502–1517. https://doi.org/10.1016/S0140-6736(08)61620-7

Deoni, S. C. L. (2007). High-resolution T1 mapping of the brain at 3T with driven equilibrium single pulse observation of T1 with high-speed incorporation of RF field inhomogeneities (DESPOT1-HIFI). *Journal of Magnetic Resonance Imaging*, *26*(4), 1106–1111. https://doi.org/10.1002/jmri.21130

Deoni, S. C. L., Matthews, L., & Kolind, S. H. (2013). One component? Two components? Three? The effect of including a nonexchanging "free" water component in multicomponent driven equilibrium single pulse observation of T1 and T2. *Magnetic Resonance in Medicine*, *70*(1), 147–154. https://doi.org/10.1002/mrm.24429

Deoni, S. C. L., Rutt, B. K., & Peters, T. M. (2003). Rapid combined T1 and T2 mapping using gradient recalled acquisition in the steady state. *Magnetic Resonance in Medicine*, *49*(3), 515–526. https://doi.org/10.1002/mrm.10407

Deoni, S. C. L., Rutt, B. K., Arun, T., Pierpaoli, C., & Jones, D. K. (2008). Gleaning multicomponent T1 and T2 information from steady-state imaging data. *Magnetic Resonance in Medicine*, *60*(6), 1372–1387. https://doi.org/10.1002/mrm.21704

Deoni, S. C. L., Ward, H. A., Peters, T. M., & Rutt, B. K. (2004). Rapid T2 estimation with phase-cycled variable nutation steady-state free precession. *Magnetic Resonance in Medicine*, *52*(2), 435–439. https://doi.org/10.1002/mrm.20159

Filippi, M., Rocca, M. A., Barkhof, F., Brück, W., Chen, J. T., Comi, G., DeLuca, G., De Stefano, N., Erickson, B. J., Evangelou, N., Fazekas, F., Geurts, J. J., Lucchinetti, C., Miller, D. H., Pelletier, D., Popescu, B. F. G., & Lassmann, H. (2012). Association between pathological and MRI findings in multiple sclerosis. *The Lancet Neurology*, *11*(4), 349–360. https://doi.org/10.1016/S1474-4422(12)70003-0

Frischer, J. M., Bramow, S., Dal-Bianco, A., Lucchinetti, C. F., Rauschka, H., Schmidbauer, M., Laursen, H., Sorensen, P. S., & Lassmann, H. (2009). The relation between inflammation and neurodegeneration in multiple sclerosis brains. *Brain*, *132*(5), 1175–1189. https://doi.org/10.1093/brain/awp070

Gelineau-Morel, R., Tomassini, V., Jenkinson, M., Johansen-Berg, H., Matthews, P. M., & Palace, J. (2012). The effect of hypointense white matter lesions on automated gray matter segmentation in multiple sclerosis. *Human Brain Mapping*, *33*(12), 2802–2814. https://doi.org/10.1002/hbm.21402

Gentile, G., Mattiesing, R. M., Brouwer, I., van Schijndel, R. A., Uitdehaag, B. M. J., Twisk, J. W. R., Kappos, L., Freedman, M. S., Comi, G., Jack, D., Barkhof, F., De Stefano, N., Vrenken, H., & Battaglini, M. (2023). The spatio-temporal relationship between concurrent lesion and brain atrophy changes in early multiple sclerosis: A post-hoc analysis of the REFLEXION study. *NeuroImage: Clinical*, *38*, 103397. https://doi.org/10.1016/j.nicl.2023.103397

Golub, M., Neto Henriques, R., & Gouveia Nunes, R. (2021). Free-water DTI estimates from single b-value data might seem plausible but must be interpreted with care. *Magnetic Resonance in Medicine*, *85*(5), 2537–2551. https://doi.org/10.1002/mrm.28599

Granberg, T., Moridi, T., Brand, J. S., Neumann, S., Hlavica, M., Piehl, F., & Ineichen, B. V. (2020). Enlarged perivascular spaces in multiple sclerosis on magnetic resonance imaging: A systematic review and meta-analysis. *Journal of Neurology*, *267*(11), 3199–3212. https://doi.org/10.1007/s00415-020-09971-5

Gross, J., & Ligges, U. (2015). nortest: Tests for Normality (1.0-4) [Computer software]. Retrieved from https://CRAN.R-project.org/package=nortest

Hasan, K. M., Gupta, R. K., Santos, R. M., Wolinsky, J. S., & Narayana, P. A. (2005). Diffusion tensor fractional anisotropy of the normal-appearing seven segments of the corpus callosum in healthy adults and relapsing-remitting multiple sclerosis patients. *Journal of Magnetic Resonance Imaging*, *21*(6), 735–743. https://doi.org/10.1002/jmri.20296

Hoy, A. R., Koay, C. G., Kecskemeti, S. R., & Alexander, A. L. (2014). Optimization of a free water elimination two-compartment model for diffusion tensor imaging. *NeuroImage*, *103*, 323–333. https://doi.org/10.1016/j.neuroimage.2014.09.053

Jenkinson, M., Beckmann, C. F., Behrens, T. E. J., Woolrich, M. W., & Smith, S. M. (2012). Fsl. *NeuroImage*, *62*(2), 782–790. https://doi.org/10.1016/j.neuroimage.2011.09.015

Klein, S., Staring, M., Murphy, K., Viergever, M. A., & Pluim, J. P. W. (2010). Elastix: A toolbox for intensity-based medical image registration. *IEEE Transactions on Medical Imaging*, *29*(1), 196–205. https://doi.org/10.1109/TMI.2009.2035616

Kurtzke, J. F. (1983). Rating neurologic impairment in multiple sclerosis: An expanded disability status scale (EDSS). *Neurology*, *33*(11), 1444. https://doi.org/10.1212/WNL.33.11.1444

Laule, C., Vavasour, I. M., Kolind, S. H., Traboulsee, A. L., Moore, G. R. W., Li, D. K. B., & MacKay, A. L. (2007). Long T2 water in multiple sclerosis: What else can we learn from multi-echo T2 relaxation? *Journal of Neurology*, *254*(11), 1579–1587. https://doi.org/10.1007/s00415-007-0595-7

Lipp, I., Foster, C., Stickland, R., Sgarlata, E., Tallantyre, E. C., Davidson, A. E., Robertson, N. P., Jones, D. K., Wise, R. G., & Tomassini, V. (2021). Predictors of training-related improvement in visuomotor performance in patients with multiple sclerosis: A behavioural and MRI study. *Multiple Sclerosis Journal*, *27*(7), 1088–1101. https://doi.org/10.1177/1352458520943788

Lipp, I., Jones, D. K., Bells, S., Sgarlata, E., Foster, C., Stickland, R., Davidson, A. E., Tallantyre, E. C., Robertson, N. P., Wise, R. G., &

Tomassini, V. (2019). Comparing MRI metrics to quantify white matter microstructural damage in multiple sclerosis. *Human Brain Mapping*, *40*(10), 2917–2932. https://doi.org/10.1002/hbm.24568

Mackay, A., Whittall, K., Adler, J., Li, D., Paty, D., & Graeb, D. (1994). In vivo visualization of myelin water in brain by magnetic resonance. *Magnetic Resonance in Medicine*, *31*(6), 673–677. https://doi.org/10.1002/mrm.1910310614

Mori, S., Wakana, S., van Zijl, P. C. M., & Nagae-Poetscher, L. M. (2005). *MRI atlas of human white matter*. Elsevier.

Parmenter, B. A., Weinstock-Guttman, B., Garg, N., Munschauer, F., & Benedict, R. H. B. (2007). Screening for cognitive impairment in multiple sclerosis using the symbol digit modalities test. *Multiple Sclerosis*, *13*(1), 52–57. https://doi.org/10.1177/1352458506070750

Pasternak, O., Sochen, N., Gur, Y., Intrator, N., & Assaf, Y. (2009). Free water elimination and mapping from diffusion MRI. *Magnetic Resonance in Medicine*, *62*(3), 717–730. https://doi.org/10.1002/mrm.22055

Piantino, J., Boespflug, E. L., Schwartz, D. L., Luther, M., Morales, A. M., Lin, A., Fossen, R. V., Silbert, L., & Nagel, B. J. (2020). Characterization of MR imaging-visible perivascular spaces in the white matter of healthy adolescents at 3T. *AJNR. American Journal of Neuroradiology*, *41*(11), 2139–2145. https://doi.org/10.3174/ajnr.A6789

Pierpaoli, C., & Jones, D. K. (2004). Removing CSF contamination in brain DT-MRIs by using a two-compartment tensor model. 1.

R Core Team. (2022). *R: A language and environment for statistical computing*. R Foundation for Statistical Computing. Retrieved from https://www.R-project.org/

Ricigliano, V. A. G., Tonietto, M., Hamzaoui, M., Poirion, É., Lazzarotto, A., Bottlaender, M., Gervais, P., Maillart, E., Stankoff, B., & Bodini, B. (2022). Spontaneous remyelination in lesions protects the integrity of surrounding tissues over time in multiple sclerosis. *European Journal of Neurology*, *29*(6), 1719–1729. https://doi.org/10.1111/ene.15285

Saade, C., Bou-Fakhredin, R., Yousem, D. M., Asmar, K., Naffaa, L., & El-Merhi, F. (2018). Gadolinium and multiple sclerosis: Vessels, barriers of the brain, and glymphatics. *AJNR: American Journal of Neuroradiology*, *39*(12), 2168–2176. https://doi.org/10.3174/ajnr.A5773

Sahraian, M. A., Radue, E.-W., Haller, S., & Kappos, L. (2010). Black holes in multiple sclerosis: Definition, evolution, and clinical correlations. *Acta Neurologica Scandinavica*, *122*(1), 1–8. https://doi.org/10.1111/j.1600-0404.2009.01221.x

Smith, S. M., Jenkinson, M., Woolrich, M. W., Beckmann, C. F., Behrens, T. E. J., Johansen-Berg, H., Bannister, P. R., De Luca, M., Drobnjak, I., Flitney, D. E., Niazy, R. K., Saunders, J., Vickers, J., Zhang, Y., De Stefano, N., Brady, J. M., & Matthews, P. M. (2004). Advances in functional and structural MR image analysis and implementation as FSL. *NeuroImage*, *23*(Suppl 1), S208–S219. https://doi.org/10.1016/j.neuroimage.2004.07.051

Smith, S. M., Zhang, Y., Jenkinson, M., Chen, J., Matthews, P. M., Federico, A., & De Stefano, N. (2002). Accurate, robust, and automated longitudinal and cross-sectional brain change analysis. *NeuroImage*, *17*(1), 479–489. https://doi.org/10.1006/nimg.2002.1040

Sumowski, J. F., Benedict, R., Enzinger, C., Filippi, M., Geurts, J. J., Hamalainen, P., Hulst, H., Inglese, M., Leavitt, V. M., Rocca, M. A., Rosti-Otajarvi, E. M., & Rao, S. (2018). Cognition in multiple sclerosis. *Neurology*, *90*(6), 278–288. https://doi.org/10.1212/WNL.0000000000004977

Tomassini, V., & Palace, J. (2009). Multiple sclerosis lesions: Insights from imaging techniques. *Expert Review of Neurotherapeutics*, *9*(9), 1341–1359. https://doi.org/10.1586/ern.09.83

Valizadeh, A., Moassefi, M., Barati, E., Ali Sahraian, M., Aghajani, F., & Fattahi, M.-R. (2021). Correlation between the clinical disability and T1 hypointense lesions' volume in cerebral magnetic resonance imaging of multiple sclerosis patients: A systematic review and meta-analysis. *CNS Neuroscience & Therapeutics*, *27*(11), 1268–1280. https://doi.org/10.1111/cns.13734

van Waesberghe, J. H., van Walderveen, M. A., Castelijns, J. A., Scheltens, P., Lycklama à Nijeholt, G. J., Polman, C. H., & Barkhof, F. (1998). Patterns of lesion development in multiple sclerosis: Longitudinal observations with T1-weighted spin-echo and magnetization transfer MR. *AJNR: American Journal of Neuroradiology*, *19*(4), 675–683.

van Walderveen, M. A. A., Lycklama à Nijeholt, G. J., Adèr, H. J., Jongen, P. J. H., Polman, C. H., Castelijns, J. A., & Barkhof, F. (2001). Hypointense lesions on T1-weighted spin-echo magnetic resonance imaging: Relation to clinical characteristics in subgroups of patients with multiple sclerosis. *Archives of Neurology*, *58*, 76–81. https://doi.org/10.1001/archneur.58.1.76

Whittall, K. P., Mackay, A. L., Graeb, D. A., Nugent, R. A., Li, D. K. B., & Paty, D. W. (1997). In vivo measurement of T2 distributions and water contents in normal human brain. *Magnetic Resonance in Medicine*, *37*(1), 34–43. https://doi.org/10.1002/mrm.1910370107

Zhang, X., Zhang, F., Huang, D., Wu, L., Ma, L., Liu, H., Zhao, Y., Yu, S., & Shi, J. (2017). Contribution of gray and white matter abnormalities to cognitive impairment in multiple sclerosis. *International Journal of Molecular Sciences*, *18*(1), 46. https://doi.org/10.3390/ijms18010046

SUPPORTING INFORMATION

Additional supporting information can be found online in the Supporting Information section at the end of this article.

How to cite this article: Caporale, A. S., Chiarelli, A. M., Biondetti, E., Villani, A., Lipp, I., Di Censo, D., Tomassini, V., & Wise, R. G. (2024). Changes of brain parenchyma free water fraction reflect tissue damage and impaired processing speed in multiple sclerosis. *Human Brain Mapping*, *45*(9), e26761. https://doi.org/10.1002/hbm.26761